Selective Hydrocracking of Waste Polyolefins toward Gasoline-Range Liquid Fuels via Tandem Catalysis over a Cerium-Promoted Pt/HY Catalyst

Zhao, Pengcheng; Guo, Wenze; Gui, Zhipeng; Jiang, Jie; Zhu, Zhihua; Li, Jin Jin; Zhao, Ling; Zhou, Jian; Xi, Zhenhao

DOI
10.1021/acssuschemeng.3c04163

Publication date
2024

Document Version
Final published version

Published in
ACS Sustainable Chemistry and Engineering

ACS Sustainable Chemistry & Engineering

pubs.acs.org/journal/ascecg

Research Article

Selective Hydrocracking of Waste Polyolefins toward Gasoline-Range Liquid Fuels via Tandem Catalysis over a Cerium-Promoted Pt/HY Catalyst

Pengcheng Zhao,[#] Wenze Guo,[#] Zhipeng Gui, Jie Jiang, Zhihua Zhu, Jin-Jin Li, Ling Zhao, Jian Zhou,* and Zhenhao Xi*

Cite This: *ACS Sustainable Chem. Eng.* 2024, 12, 5738−5752

Read Online

ACCESS | Metrics & More | Article Recommendations | Supporting Information

ABSTRACT: Upcycling of waste plastics into value-added chemicals and fuels represents a promising orientation toward a more sustainable chemical industry. We present a selective process for hydrocracking waste polyolefins into a spectrum of branched gasoline-range C_{5-12} hydrocarbons, utilizing a cerium-promoted Pt/HY as a metal−acid bifunctional catalyst. The HY zeolite was engineered with a hierarchical meso/microporosity and moderated acidity to alleviate the overcracking of intermediate hydrocarbons to light C_{1-4} gas products. The cerium presented as a surface cerium oxide phase, which mitigated acidity and significantly improved Pt dispersion. Upon a proper metal−acid balance, an optimized yield of C_{5-12} up to 85 wt % was achieved from the low-density polyethylene over a cerium-promoted Pt/HY catalyst at 280 °C and 2 MPa H_2 for 2 h. The tandem catalysis was proposed to proceed with an initial dehydrogenation of the polymer chain over Pt sites, with subsequent isomerization and cracking over the Brønsted acid sites and hydrogenation of the olefin intermediates over Pt sites. The strong Pt−O−Ce bridging structure inhibited the migration and agglomeration of Pt atoms, affording good stability and no distinct performance loss over three sequential runs. This process is applicable to the hydrocracking of other polyolefins such as high-density polyethylene, polypropylene, and daily plastic bags to gasoline-range fuels in desirable yields (60−80 wt %).

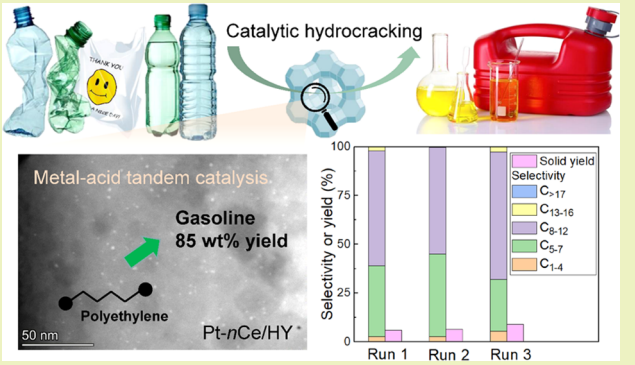

KEYWORDS: *polyolefin, hydrocracking, bifunctional catalyst, platinum, cerium oxide, gasoline*

INTRODUCTION

Plastics play an essential role in modern life due to their low cost and desirable physiochemical properties. In 2021, the global plastic production reached 390.7 million tons and is projected to increase to 1200 million tons by 2050.[1] The large plastic production and usage has led to enormous plastic waste, of which only 8.8% is currently recycled (physically), while the rest is mainly disposed in landfills or directly incinerated,[2,3] causing severe economic loss and environmental problem. Considering also the depleting fossil reserves and the popularity of exploiting sustainable alternative resources (e.g., lignocellulosic biomass),[4−7] upcycling of waste plastics, e.g., polyolefins (PO), which takes up the largest fraction of the waste plastics, into value-added chemicals and fuels represents a promising direction toward a greener chemical industry and circular economy and thus has received significant research attention.[8−10]

Compared to mechanical recycling, which usually leads to lower-value products, chemical conversion of waste PO is a more versatile and promising approach, with which a spectrum of fuel-range hydrocarbons could be produced upon proper catalysts and process conditions. Thermal or catalytic pyrolysis, as well as catalytic hydrogenolysis and hydrocracking, are the main methods for the chemical recovery of PO. Representative literature studies on the chemical conversion of polyethylene are summarized in Table 1. Wax, benzene, toluene and xylene (BTX), and light olefins could be produced from PO pyrolysis at 400−900 °C.[11−15] Amorphous SiO_2−Al_2O_3 and zeolites (e.g., HY and HZSM-5) are often used as catalysts for pyrolysis,[16−23] which gave certain yields of gasoline or diesel-range hydrocarbons, as well as high fractions of light C_{1-4} hydrocarbons, tar, and coke (cf. entries 1−7 of Table 1). High temperatures (>400 °C) are required for the pyrolysis in order to supply sufficient energy for the cleavage of the C−C bonds,[24,25] which tend to cause a low selectivity of the desired

Received: July 12, 2023
Revised: February 23, 2024
Accepted: February 26, 2024
Published: March 15, 2024

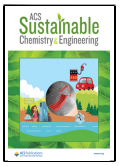

https://doi.org/10.1021/acssuschemeng.3c04163
ACS Sustainable Chem. Eng. 2024, 12, 5738−5752

Table 1. Overview of Representative Literature Studies on the Chemical Conversion of Polyethylene (PE)

				reaction conditions			product yield		
entry	feed	method	catalyst	temperature (°C)	H_2 pressure (MPa)	time	solid (wt %)	hydrocarbons[b]	[b]refs
1	HDPE	pyrolysis		515		4.6 s[a]	0.2	2.5 wt % gas (C_{1-4}), 10.5 wt % oil (C_{5-20}), 86.6 wt % wax ($C_{>20}$)	11
2	PE	pyrolysis		800		1.0−10 s[a]	[c]	84.3 wt % (gas), 15.3 wt % (oil)	36
3	LDPE	pyrolysis		780−825		0.4−0.6 s[a]		88.0−92.9 wt % (gas) 5.0−8.0 wt % (oil)	37
4	PE	pyrolysis	amorphous SiO_2−Al_2O_3 + HZSM-5	375		7 min g of catalyst/g of PE		58.8 wt % gasoline C_{5-12} (25.2 aromatics and 0.9% benzene)	21
5	HDPE	pyrolysis	HZSM-5	620		90 s		49 wt % gas, 35.9 wt % gasoline C_{5-12} (45% aromatics and 24.6% isomerized aliphatic)	22
6	LDPE	pyrolysis	HY	350−375		200 s		88 mol % olefins	23
7	HDPE	pyrolysis	Ru/HY	600		0.5 h		32.30 wt % (aromatics)	38
8	PE	hydrogenolysis	Pt/$SrTiO_3$	300	1.2	96 h	0	>99 wt % liquid products (lubricants and waxes)	33
9	LDPE	hydrogenolysis	Ru/CeO_2	240	6	8 h		9.7 mol % gas (C_{1-4}), 22 mol % gasoline (C_{5-10}), 62 mol % diesel (C_{10-21}), wax (C_{22-45})	35
10	HDPE	hydrogenolysis	*m*SiO_2/Pt/SiO_2	300	1.38	48 h		38 wt % diesel (C_{12-16})	39
11	LDPE	hydrocracking	Pt@S-1 + H-*β*	250	3	2 h	0.5	89.5 wt % liquid (96.8% selectivity of C_{5-9})	40
12	LDPE	hydrocracking	Pt/H-*β*	330	2	1 h	0	45 wt % gas (C_{1-4}) and 39 wt % gasoline (C_{5-12})	41
13	LDPE	hydrocracking	Pt/H-USY	260	6	42 h		19 mol % gas (C_{1-4}), 80 mol % gasoline (C_{5-10}), 2.2 mol % diesel (C_{10-21}), <0.1 mol % wax (C_{22-45})	35
14	LDPE	hydrocracking	Pt/WO_3/ZrO_2 + HY	225	3	2 h	6	8.1 mol % gas (C_{1-4}), 73 mol % gasoline (C_{5-12}), 20 mol % diesel (C_{9-22})	42
15	LDPE	hydrocracking	Pt/HY	280	2	2 h	9.7	4.3 wt % gas (C_{1-4}), 81.4 wt % gasoline (C_{5-12})	this work
16	LDPE	hydrocracking	Pt-3Ce/HY	280	2	2 h	5.1	2.6 wt % gas (C_{1-4}), 84.8 wt % gasoline (C_{5-12}), 1.7 wt % diesel (C_{13-16})	this work

[a]Gas residence time in the fluidized bed reactor. [b]Gas/liquid product yields in entries 6, 9, 13, and 14 are on carbon basis and those in the other entries are on mass basis. [c]Not given in the literature.

https://doi.org/10.1021/acssuschemeng.3c04163
ACS Sustainable Chem. Eng. 2024, 12, 5738−5752

Table 2. Composition, Textural, and Surface Chemical Properties of Catalysts

	total content[a] (wt %)		surface content[b] (mol %)									
catalysts	Pt	Ce	Pt	Ce	S_{BET}[c] ($m^2\ g^{-1}$)	S_{micro}[c] ($m^2\ g^{-1}$)	V_{tot}[c] ($cm^3\ g^{-1}$)	V_{micro}[c] ($cm^3\ g^{-1}$)	$Pt^{2+}/(Pt^0 + Pt^{2+})$[b]	$Ce^{3+}/(Ce^{3+} + Ce^{4+})$[b]	D_{Pt}[d] (%)	d_{Pt}[e] (nm)
HY (pristine)					653	575	0.37	0.22				
HY (hierarchical)					809	656	0.44	0.26				
Pt/HY	0.46		0.67		662	501	0.40	0.20	35.0%		19.5	2.6
Pt-1Ce/HY	0.48	1.1	0.59	0.13	694	640	0.38	0.25	38.9%	25.9%	13.4	3.7
Pt-3Ce/HY	0.45	3.0	0.57	0.20	680	604	0.37	0.24	50.7%	32.4%	23.9	2.1
Pt-5Ce/HY	0.46	5.1	0.51	0.31	599	542	0.32	0.21	64.0%	40.1%	41.6	1.0
Pt-11Ce/HY	0.47	11.0	0.56	0.92	574	500	0.32	0.20	86.9%[f]	43.1%	78.9	0.4

[a]Determined by ICP-AES analysis. [b]Determined by XPS. [c]S_{BET} and V_{tot} denote the BET specific surface area and total pore volume; S_{micro} and V_{micro} denote the surface area and volume of micropores, respectively. [d]Dispersion of active Pt sites, which is determined by CO-pulse chemisorption; the calculation details are given in Section S1.3. [e]Pt crystallite size, which is determined from Pt dispersion (D_{Pt}) according to the literature.[5555] [f]Determined by $(Pt^{2+} + Pt^{4+})/(Pt^0 + Pt^{2+} + Pt^{4+})$.

products (e.g., due to the overcracking) and fast catalyst deactivation (e.g., by severe coke deposition). Comparatively, metal-catalyzed hydrogenolysis has been reported to be effective for PO breakdown at relatively lower temperatures (ca. 300 °C) with a low generation of the coke precursor in the hydrogen atmosphere.[26,27] Due to the structural similarity between PO and *n*-alkanes, PO hydrogenolysis may be guided to some extent by the principle governing hydrogenolysis of *n*-alkanes. Iglesia et al. extensively studied the catalytic hydrogenolysis of C_2-C_{10} alkanes over supported Pt, Ir, Ru, and Rh metals,[28−32] and the catalytic performance is found to be related to multiple factors such as the operating conditions (temperature and H_2 pressure), the properties of supported metal particles (size and metal type), and the degree of carbon atom substitution of *n*-alkanes. Celik et al. reported the production of lubricating oil and wax over a $Pt/SrTiO_3$ catalyst at 300 °C, 1.2 MPa H_2, and 96 h, with a yield of 42 to >99 wt % depending on the properties of polyethylene feedstocks.[33] Zhang et al. achieved the direct transformation of polyethylene to long-chain alkylaromatics via Pt-catalyzed tandem hydrogenolysis/aromatization over a $Pt/\gamma\text{-}Al_2O_3$ catalyst under hydrogen-free conditions.[34] Nakaji et al. reported the hydrogenolysis of low-density polyethylene (LDPE) to C_{5-21} liquid fuel over a Ru/CeO_2 catalyst with a yield of 88 mol % (carbon basis) at 240 °C, 6 MPa H_2 for 8 h.[35] Notably, due to the lack of acid sites for carbon bone isomerization on the monofunctional metal catalysts, most of the hydrogenolysis products are short of chain branching and have a relatively high melting point (>room temperature) that limits their direct applications. In addition, the hydrogenolysis reaction usually requires long reaction times, high temperatures (>300 °C), or high catalyst loadings (cf. entries 5−7 of Table 1).

Comparatively, hydrocracking over bifunctional metal/acid catalysts at moderate temperatures and H_2 pressures have appeared to be a more promising approach, where the acid catalyst cracks C−C bonds, and the metal catalyst hydrogenates the olefin intermediates, suppressing the coke formation. Most reported PO hydrocracking studies have focused on the metals (e.g., Pt, Pd, Ni, Co, Ru) supported on microporous zeolites (e.g., HY, HZSM-5), which however behave unselective conversion toward C_{1-4} light gas due to the severe overcracking (cf. entries 8 and 9 of Table 1).[26,41,43−45] Concretely, most of the reaction intermediates, which were initially produced from Pt-catalyzed dehydrogenation or hydrogenolysis, are confined in the zeolite microporous network, where the larger hydrocarbons face severe diffusion limitations and thus undergo deep cracking to smaller products.[46] Vlachos' group recently reported the hydrocracking of LDPE using a blend of $Pt/WO_3/ZrO_2$ and HY zeolite as the catalysts.[46] In this way, the Pt sites were separated from the strong acid sites on the microporous HY zeolites, alleviating the overcracking and increasing the yields of medium- and high-range fuel products, giving a C_{5-22} liquid fuel yield of 85 mol % (carbon basis) at 250 °C and 3 MPa H_2 for 2 h. Generally, the hydrocracking of PO proceeds via synergistic metal−acid catalysis that involves the initial activation of PO and the hydrogenation of olefin intermediates over the metal catalysts, and a series of cracking and isomerization reactions over the acid sites.[46] As such, a proper balance between metal and acid catalysis is required for the efficient PO hydrocracking, which should enable a high conversion rate of PO without overcracking the valuable fuel-range C_{5-22} products. Shape selectivity, in addition to metal and acid catalysis, also plays an important role in the PO hydrocracking, as the slower diffusion of the reaction intermediates in zeolites with narrower pores would facilitate their overcracking. Therefore, engineering the acidity and porosity of the zeolite is crucial for the selective PO conversion to the desired products. In addition, the hydrocracking catalysts tend to deactivate due to the metal migration/agglomeration, zeolite dealumination, or coke deposit covering metal and acid sites; as such, the stability and reusability should be well-addressed in the catalyst/process development.

In this work, a cerium-promoted hierarchical Pt/HY catalyst was synthesized and applied in the catalytic hydrocracking of PO. Pt metal was supported on a hierarchically porous HY zeolite, which was engineered via partial dealumination/desilication in order to alleviate the acidity and create additional mesoporosity in the HY framework. Cerium oxide was added aiming to regulate the acidity, improve the Pt dispersion, and inhibit the agglomeration of Pt particles via the formation of a stable Pt−O−Ce bridging structure.[47−50] The physiochemical properties of the catalysts were characterized systematically, and the catalytic performance was evaluated in the hydrocracking of LDPE under a wide range of reaction conditions (temperature and H_2 pressure). Furthermore, the process/catalyst was extended to other polyolefins such as high-density polyethylene (HDPE), polypropylene (PP), and

https://doi.org/10.1021/acssuschemeng.3c04163
ACS Sustainable Chem. Eng. 2024, 12, 5738−5752

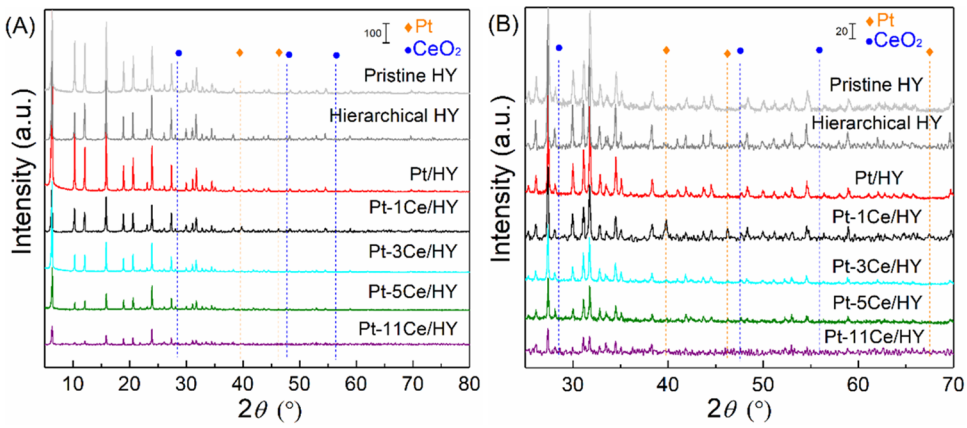

Figure 1. (A) XRD patterns of HY, Pt/HY, and Pt-*n*Ce/HY catalysts and (B) magnified view of the XRD patterns at the 2θ region of 25−70°.

recycled commercial plastic bags (consisting of HDPE) under the optimized catalyst and reaction conditions. Mechanistic insights into the metal−acid tandem catalysis for PO hydrocracking was elucidated based on the experimental findings and literature studies, and the stability and reusability of the catalyst were evaluated.

RESULTS AND DISCUSSION

The (cerium-promoted) Pt/HY catalysts were synthesized via a simple incipient wetness impregnation method using a custom-modified HY zeolite as the support. Briefly, an aqueous solution of $Ce(NO_3)_3{\cdot}6H_2O$ and $H_2PtCl_6{\cdot}6H_2O$ was used to impregnate the HY zeolites at room temperature for 24 h. Afterward, the as-prepared catalysts were vacuum-dried at 120 °C overnight followed by calcination in the air at 550 °C for 6 h and reduction in a hydrogen flow at 50 mL/min and 300 °C for 4 h. The synthesized catalysts were denoted as Pt-*n*Ce/HY catalysts, where *n* (= 1, 2, 3, 4, 5 or 11) denotes the weight percent (wt %) of the Ce elements. For all catalysts, the Pt loading is 0.5 wt %. The details regarding the materials, catalyst synthesis, characterizations, and calculations are given in Section S1.

Crystalline Structure, Textural Properties, and Pt Dispersion. The contents of Pt and Ce in the catalysts were confirmed by inductively coupled plasma-atomic emission spectroscopy (ICP-AES) analysis (Table 2), and the results agree well with the calculated value in the sample synthesis, suggesting the successful loading of Pt and Ce by the applied impregnation method. The crystalline structure of the pristine HY, hierarchical HY zeolite, and Pt/HY and Pt-*n*Ce/HY catalysts was investigated by wide-angle X-ray diffraction (XRD), as shown in Figure 1A,B. The pristine HY and hierarchical HY displayed highly similar XRD patterns, indicating an almost unchanged crystallinity of the HY zeolite upon modification. The patterns of all Pt/HY and Pt-*n*Ce/HY catalysts display the characteristic diffraction peaks of the HY zeolite, which decreased gradually in intensity with the increased loading of Pt or Ce. The Pt/HY exhibited three characteristic peaks of Pt crystalline at 2θ = 39.8, 46.2, and 67.5°.[51] The intensity of these peaks first increased with the addition of 1 wt % Ce (i.e., Pt-1Ce/HY) and then decreased gradually with further increase of Ce loading to 3 wt % (Figure 1). The Pt-5Ce/HY and Pt-11Ce/HY catalysts gave no distinct diffraction peaks for Pt crystalline, indicating an even smaller Pt particle size that is below the detection limit of XRD. The decreased peak intensity of Pt crystalline suggested an inhibited growth of Pt particles and suppressed formation of the three-dimensional (3D) bulk Pt crystalline, inferring an improved Pt dispersion upon the proper addition of Ce (i.e., >1 wt %). For all Pt-*n*Ce/HY samples, no distinct diffraction peak of CeO_2 (2θ = 28.5, 47.5, and 56.3°[51]) was observed in the pattern, indicating the absence of CeO_2 crystalline or an amorphous nature of cerium oxide (vide infra).

The textural properties of the catalysts were studied by N_2 sorption, as shown in Figure S4 and Table 2. All of the samples exhibited a type I isotherm and an H4-type hysteresis loop (Figure S4A). The density functional theory (DFT) pore size distribution indicated the copresence of meso- (2−40 nm) and micropores (0.5−1 nm; cf. Figure S4B,C), which corroborates the hierarchical meso/microporosity of the custom-modified HY zeolite and the synthesized Pt/HY and Pt-*n*Ce/HY catalysts. Notably, a certain extent of mesoporosity was already found in the pristine HY zeolite (Figure S4 and Table 2), which is consistent with the literature findings.[42] Upon modification, the mesoporosity of the HY zeolite was further promoted; e.g., as shown in Figure S4C, more pores of ca. 2−30 nm were generated compared to pristine HY zeolite. A logical decreasing trend was observed in the specific surface area (S_{BET}) and pore volume (V_{tot}) with the increase of the loading of Pt or Ce, due to the gradual occupancy of the inner pores of the catalysts (Table 2). For example, the specific surface area of the HY zeolite decreased from 809.06 to 737.51 m^2/g after loading with 0.5 wt % Pt, which was further decreased gradually to 573.64 m^2/g after the increase of Ce loading up to 11 wt %. Similarly, the pore volume of HY zeolite decreased from 0.44 to 0.32 cm^3/g after the loading of 0.5 wt % Pt and 11 wt % Ce (i.e., Pt-11Ce/HY).

The dispersion of Pt in Pt/HY and Pt-*n*Ce/HY catalysts was evaluated using a CO-pulse adsorption method (Table 2). The results show that the dispersion of Pt (D_{Pt}) first decreased with the addition of 1 wt % Ce, which is attributed to the surface occupancy by CeO_2, leading to a reduced free surface area for Pt dispersion and thus the partial agglomeration of Pt. With the further increase of Ce addition, more CeO_2 phase (together with the oxygen vacancies) was generated, and the dispersion of Pt improved significantly, e.g., from 13.4% for Pt-1Ce/HY to 78.9% for Pt-11Ce/HY. The Pt crystallite size estimated from the Pt dispersion gave an opposite evolution trend with increasing Ce loading (Table 2). CeO_2 has been known with its abundant surface oxygen vacancies, which tend to adsorb the Pt species and promote the dispersion of Pt particles on the CeO_2 surface.[52−54] In addition, the CeO_2

https://doi.org/10.1021/acssuschemeng.3c04163
ACS Sustainable Chem. Eng. 2024, 12, 5738−5752

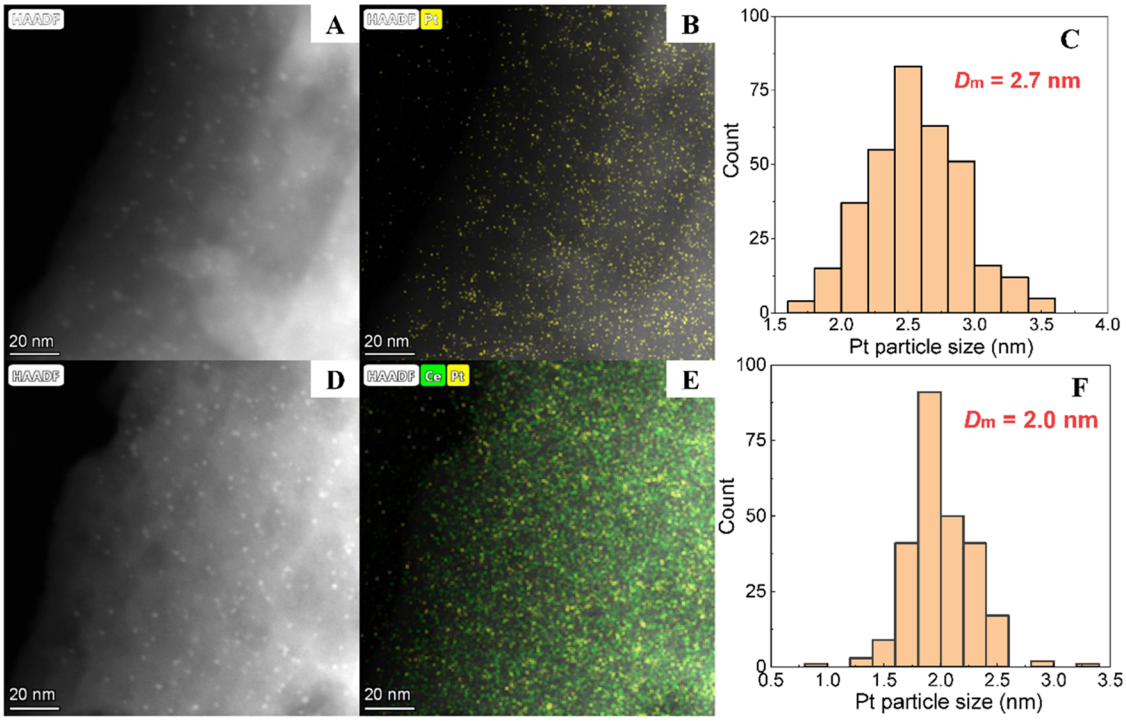

Figure 2. HAADF-STEM images, the corresponding EDS elemental mapping, and the Pt particle size distribution of (A−C) Pt/HY and (D−F) Pt-3Ce/HY. The STEM images used for Pt size determination are given in Figures S5 and S6. The D_m in parts (C, F) denote the average size of the Pt particles.

phase also acts as a diffusion barrier that prevents the aggregation of the Pt species on the HY support. As such, Pt dispersion was largely improved upon a relatively high Ce addition (e.g., >3 wt %). These findings on Pt dispersion are consistent with the evolution of the Pt diffraction peak intensity with increasing Ce loading as revealed by the wide-angle XRD (Figure 1).

The morphology and dispersion of Pt particles were further investigated by high-angle annular dark-field scanning transmission electron microscopy (HAADF-STEM) as well as the corresponding element mapping, using Pt-HY and Pt/3Ce-HY catalysts as examples (Figure 2). The STEM image of Pt/HY indicated the uniform distribution of fine Pt particles (<4 nm) on the surface (Figure 2A,B), giving a relatively wide distribution of the Pt particle size and an average value (D_m) of about 2.7 nm (Figure 2C). Similar fine Pt particles were also observed on Pt/3Ce-HY (Figure 2D,E), which are uniformly dispersed together with CeO_2 throughout the support (Figure 2E), affording a narrow distribution of the Pt particle size with an average value (D_m) of ca. 2.0 nm (Figure 2F). These values agree well with that estimated from Pt dispersions (being 2.6 nm for Pt/HY and 2.1 nm for Pt-3Ce/HY; cf. Table 2). Generally, the promoting effect of CeO_2 on Pt dispersion was clearly reflected on the STEM/energy dispersive spectroscopy (STEM/EDS) images, in line with the results of XRD and CO-pulse adsorption.

Surface Chemical Properties. X-ray photoelectron spectroscopy (XPS) characterizations were performed on Pt/HY and Pt-*n*Ce/HY catalysts to gain insights into the chemical state of the surface Pt and Ce atoms that is strongly related to their catalytic performance (Figures 3 and S7 and Tables S1 and S2). For all samples (except Pt-11Ce/HY), the Pt $4f_{5/2}$ region is fitted as two peaks at 74.2 and 76.1 eV (Figure 3A−D), suggesting two different chemical states of the surface Pt atoms, i.e., the peak at 74.2 eV corresponds to Pt^0, while the other one at 76.1 eV belongs to Pt^{2+}.[56] Apparently, the majority of Pt on the Pt/HY catalyst exists in the form of Pt^0, as the content of Pt^0 accounts for ca. 65% of the overall surface Pt atoms on Pt/HY. With the addition of Ce, the portion of Pt^{2+} increased gradually, from 35% for Pt/HY to 64% for Pt-5Ce/HY (Table 2). For Pt-11Ce/HY, a new peak appeared at ca. 78.3 eV in the $4f_{5/2}$ region, which is assigned to Pt^{4+} and the portion of electron-deficient Pt atoms (Pt^{2+} + Pt^{4+}) takes up 86.9% (Figure 3E and Table 2). Similar peak distributions and intensity evolutions were also observed for Pt $4f_{7/2}$ peaks for all samples. Such an increased electron-deficient state of Pt is attributed to an enhanced electron transfer from Pt to Ce (e.g., $Pt^0 + Ce^{4+} \rightarrow Pt^{2+} + Ce^{3+}$) via an increased formation of Pt−O−Ce bridging structure at higher Ce loadings.[57] This is somewhat supported by the evolution of the chemical state of Ce ions. As shown in Figure S7, among the deconvoluted peaks of the XPS spectra of Ce $3d_{3/2}$, the peaks at ca. 897.1 and 901.9 eV are assigned to Ce^{3+}, and the remaining several deconvoluted peaks at 899.6, 905.9, and 915.3 eV are characteristic of Ce^{4+}.[58−61] This also indicates that the Ce element is present as a cerium oxide in the Pt-*n*Ce/HY catalysts. It is observed that the portion of Ce^{3+} increased with the increase of Ce addition, e.g., from 32.4% for Pt-3Ce/HY to 43.1% for Pt-11Ce/HY (Table 2), which is indicative of an increased electron transfer from Pt toward Ce ions, in line with the increased portion of Pt^{2+}. The peaks of Ce $3d_{5/2}$ gave a similar peak distribution and intensity evolution (Figure S7 and Table S2). Generally, XPS characterization corroborates the strong interaction between Pt and Ce via a Pt−O−Ce bridging structure, which is supposed to have a large impact on its performance in the catalytic hydrocracking of PO (vide infra).

https://doi.org/10.1021/acssuschemeng.3c04163
ACS Sustainable Chem. Eng. 2024, 12, 5738−5752

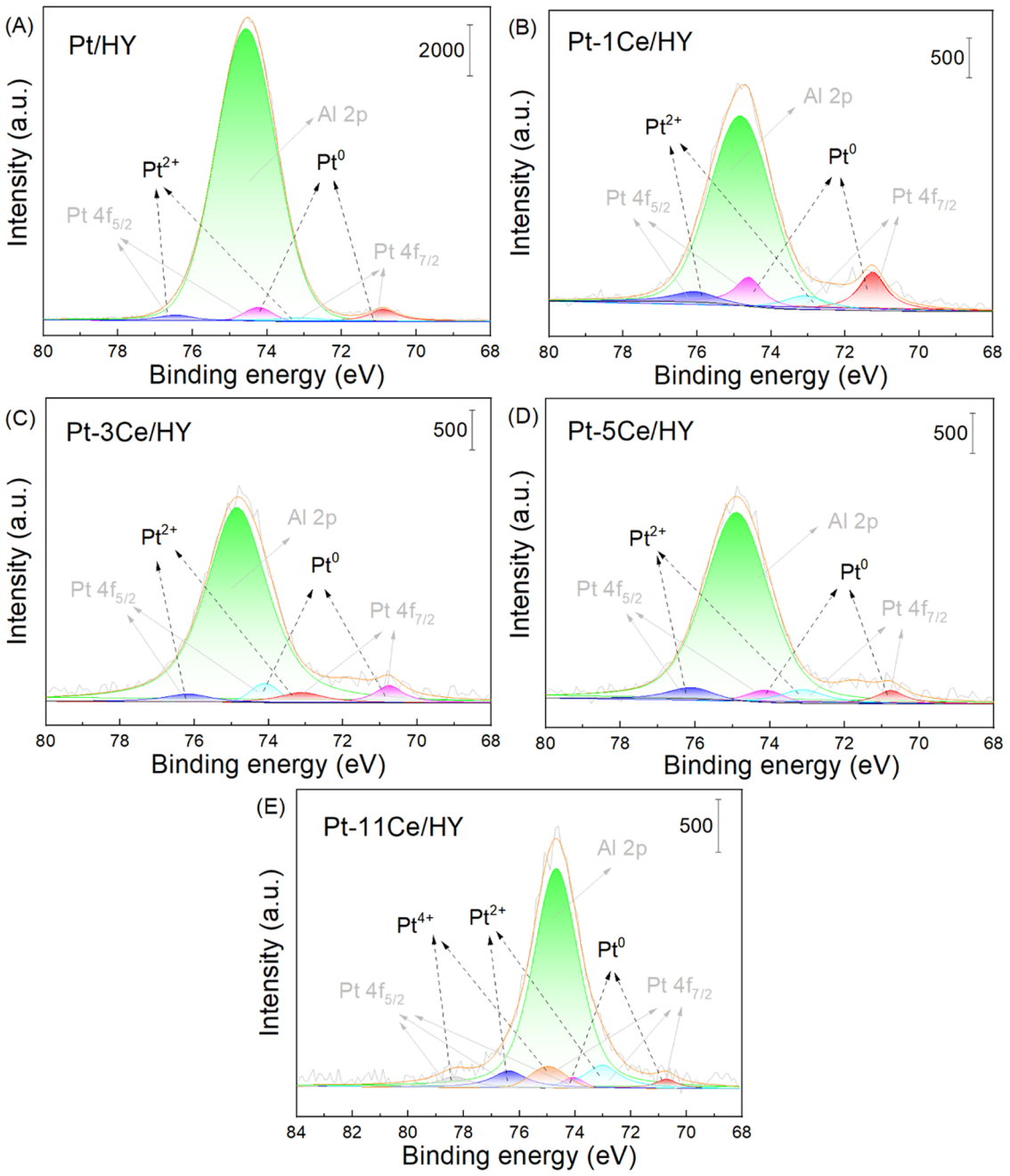

Figure 3. XPS spectra of Pt 4f on the surface of (A) Pt/HY, (B) Pt-1Ce/HY, (C) Pt-3Ce/HY, (D) Pt-5Ce/HY, and (E) Pt-11Ce/HY catalysts. The corresponding peak fitting parameters are given in Table S1.

The H_2-TPR profiles of Pt/HY, 3Ce/HY, and Pt-*n*Ce/HY catalysts are shown in Figure 4. Pure CeO_2 supported on HY (3Ce/HY) gave two reduction peaks: the small and broad reduction peak at 350−550 °C is due to the reduction of surface oxygen of CeO_2, and the other peak at a higher temperature >600 °C is assigned to the reduction of bulk CeO_2.[47,62,63] The unreduced Pt/HY displayed a relatively small wide peak at 100−300 °C and a broad peak before 550 °C. The former peak is attributed to the reduction of the large-sized PtO species (Pt^{2+} to Pt^0) located on the external surface and interacted relatively weakly with the support. The other peak at 400−550 °C is assigned to the reduction of highly dispersed PtO species (of small size) that interacted strongly with the supports and most possibly located in the inner pores. Concretely, this peak was deconvoluted into two reduction peaks at ca. 440 °C (region I) and 480 °C (region II; somewhat overlapped with the reduction peak of the surface oxygen of CeO_2), among which the peak at a higher temperature (>450 °C) is derived from the reduction of the $Pt-(O-Si\equiv)_y^{2-y}$ structure formed by the coordination between Pt and surface silanol groups (≡Si−OH) on HY zeolites.[48,64,65] Upon reduction to 300 °C, the peak at 100−300 °C disappeared reasonably for all reduced Pt/HY and Pt-*n*Ce/HY samples. After the addition of Ce, a new peak appeared at ca. 600 °C (region III), which is attributed to the reduction of the bulk ceria.[47] Compared to 3Ce/HY, this peak shifted to a lower temperature, indicating an increased reducibility of Ce^{4+} upon interaction with Pt. It was observed

https://doi.org/10.1021/acssuschemeng.3c04163
ACS Sustainable Chem. Eng. 2024, 12, 5738−5752

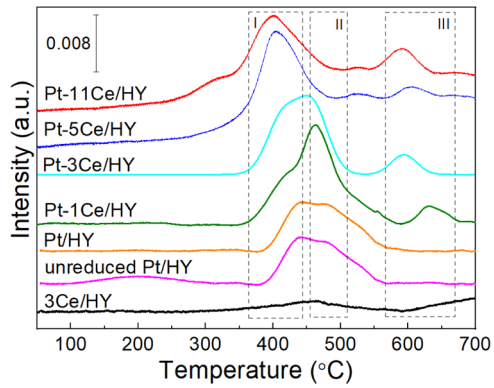

Figure 4. H_2-TPR profiles of Pt/HY, 3Ce/HY, and Pt-*n*Ce/HY catalysts. The location of the reduction peaks was divided into regions I, II, or III. The catalyst samples have been prereduced at 300 °C for 4 h before analysis (unless otherwise stated; cf. Section S1.2).

that with the increase of Ce addition, the peak of Pt^{2+} reduction at >450 °C (region II) decreased significantly in intensity and almost disappeared for Pt-5Ce/HY and Pt-11Ce/HY. This can be explained by the increased generation of the surface cerium oxide phase and the Pt−O−Ce structure at higher Ce addition leading to less formation of $Pt-(O-Si\equiv)_y^{2-y}$, in line with the XPS characterization results. The preferential interaction of Pt with Ce also infers the regulating effect of CeO_2 on the dispersion and chemical state of Pt and thus its catalytic performance in PO hydrocracking.

In tandem catalysis for PO hydrocracking, the acid sites, in addition to the Pt particles, also play a significant role. Particularly, the Brønsted acid sites (BAS) are primarily responsible for the generation of the carbocation intermediates and overall catalytic activity.[66] The types and amounts of the surface acid sites on HY, Pt/HY, and Pt-*n*Ce/HY catalysts were further determined by pyridine-IR (Figures 5, S8, and S9

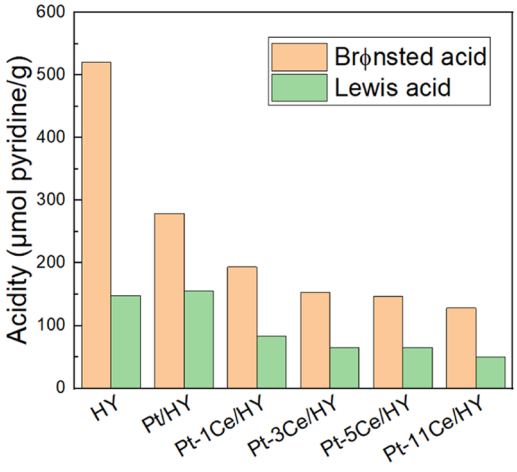

Figure 5. Acid properties of HY, Pt/HY, and Pt-*n*Ce/HY catalysts.

and Tables 3 and S3). Pure HY zeolites afford both Lewis acid sites (LAS) and BAS, with a Brønsted to Lewis acid (B/L) ratio of 3.51. After Pt loading, the amount of BAS decreased significantly, while the concentration of LAS remained almost unchanged, giving a B/L ratio of 1.80 for Pt/HY. Upon the addition of 1 wt % Ce, both LAS and BAS decreased largely, which then leveled off gradually with further increase of Ce loading, rendering the B/L ratios for the Pt-*n*Ce/HY catalysts

Table 3. Acid and Pt Densities of HY, Pt/HY, and Pt-*n*Ce/HY Catalysts

	acidity[a] (μmol pyridine/g)			
sample	Brønsted	Lewis	B/L	n_{Pt}[b] (μmol/g)
HY	520.5	148.2	3.51	
Pt/HY	279.1	154.9	1.80	5.0
Pt-1Ce/HY	193.5	83.7	2.31	3.4
Pt-3Ce/HY	152.6	64.8	2.35	6.1
Pt-5Ce/HY	146.7	65.4	2.25	10.7
Pt-11Ce/HY	128.1	50.1	2.55	20.2

[a]Determined by pyridine-IR (at an evacuation temperature of 200 °C). [b]Density of the active Pt sites, which is determined by CO-pulse chemisorption.

falling within 2.25−2.55 (Table 3). Generally, a decreasing trend was observed in the amounts of weak, moderate, and strong LAS/BAS as well as the total acidity with the increase of Ce loading (Figure 5 and Tables 3 and S3). The aforementioned variation of the acid properties of Pt-*n*Ce/HY catalysts was seen as a result of (i) the deposit of Pt and CeO_2 over HY zeolites, covering the acid sites therein and occupying the surface area of the inner pore channels and (ii) the creation of the new acid sites on the CeO_2 phase. The regulating effect of CeO_2 on the acid properties, in addition to Pt properties, again inferred its large impact on the metal−acid tandem catalysis and somewhat justified our strategy of using CeO_2 as a promoter of Pt/HY for its enhanced performance in PO hydrocracking.

Catalytic Hydrocracking of LDPE over HY, Pt/HY, and Pt-*n*Ce/HY Catalysts. Catalytic performance of HY zeolite, Pt/HY, and Pt-*n*Ce/HY catalysts in the hydrocracking of LDPE ($M_n \approx 24{,}064$ g mol^{-1}, cf. Figure S2) was studied using 200 mg of catalyst and 2.0 g of PO at a relatively mild reaction condition of 280 °C and 2 MPa H_2 for 2 h (Figure 6). The HY zeolite exhibited rather limited LDPE conversion with severe coke formation, leading to a high solid residue yield of 93 wt % (Figure 6A). Comparatively, Pt/HY afforded a much higher activity, giving only ca. 10 wt % of unconverted solid residue but 90.3 wt % of extractable (gas + liquid) products, with a narrow product distribution and high degree of chain branching (Figure 6B). Among others, the liquid products are C_{5-12} gasoline-range hydrocarbons that were attained at a relatively high yield of 81.4 wt %. Notably, Pt/HY zeolite has been commonly used in the petrochemical refinery as the catalyst for the hydrocracking of long-chain alkanes,[67] and recently has also been used in the catalytic hydrocracking of plastics.[41,43,68] However, the reported Pt/HY catalysts, which have used standard commercial HY zeolites as the support, exhibit unselective PO hydrocracking to C_{1-4} light gas products, as most of the intermediate long-chain hydrocarbons are confined in the zeolite microporous framework with large diffusional limitations, thus undergoing severe overcracking to light gases on abundant acid sites therein.[46] In this work, we have utilized a partially dealuminated/desilicated HY zeolite as the support for the synthesis of Pt/HY (as well as Pt-*n*Ce/HY) catalysts with a hierarchical meso/microporous structure and moderated acidity (cf. Tables 2 and 3), which represents an effective approach to alleviate the overcracking of medium C_{5-12} hydrocarbons. The far higher activity of Pt/HY compared to HY is attributed to the synergy of Pt and acid sites in the tandem catalysis for LDPE hydrocracking. Concretely, Pt particles are responsible for the activation of

https://doi.org/10.1021/acssuschemeng.3c04163
ACS Sustainable Chem. Eng. 2024, 12, 5738−5752

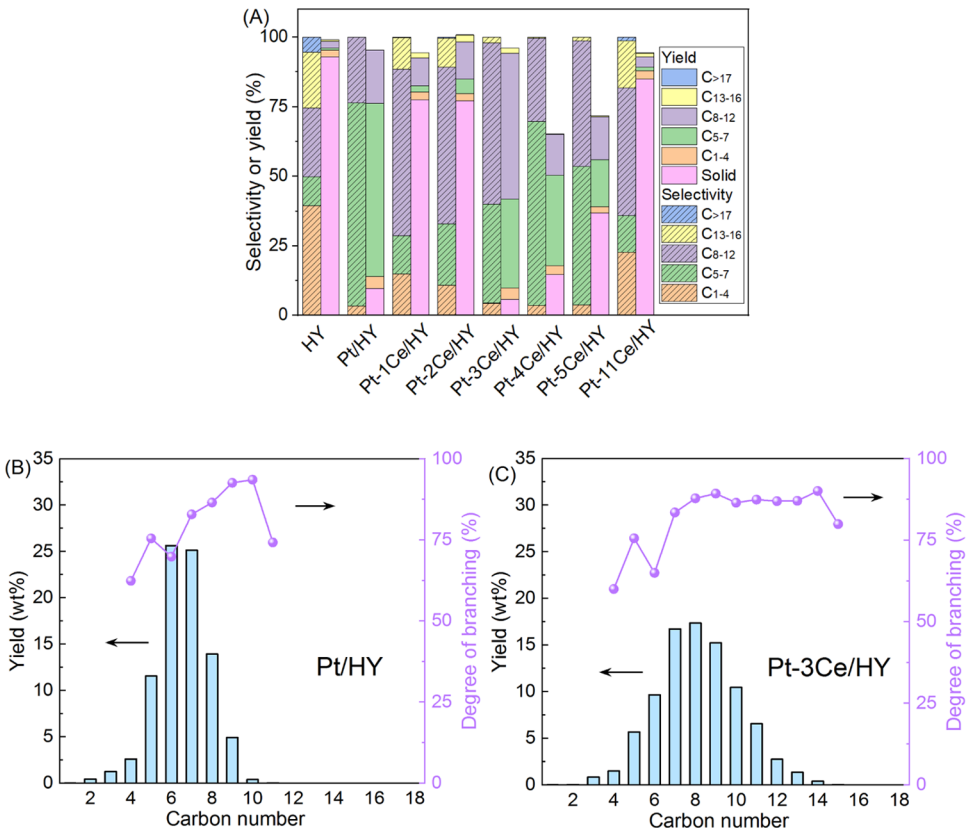

Figure 6. (A) Product selectivity and yield over HY, Pt/HY, and Pt-*n*Ce/HY catalysts under the same conditions; (B, C) product yield distribution by carbon number and the corresponding isomerization degree over (B) Pt/HY and (C) Pt-3Ce/HY catalysts. Reaction conditions: 280 °C, 2 MPa H_2, 2 h, 200 mg of catalyst, and 2.0 g of PO.

the polymer chains by converting the large $C_{>17}$ paraffins to olefins, which are then cracked into C_{13-16} over the acid sites. The produced smaller hydrocarbons then diffused into the inner meso/micropores undergoing further cracking to C_{8-12}, then to C_{5-7} hydrocarbons, and even to C_{1-4} light gases. In the meantime, the Pt particles also hydrogenate the olefin coke precursors, suppressing the coke formation.[42] The mechanistic discussion on PO hydrocracking via tandem catalysis based on the literature findings and experimental results is given in the Supporting Information (cf., Scheme S1). Notably, at the studied mild temperatures and short reaction times, Pt is active for the dehydrogenation/hydrogenation of alkane/alkene hydrocarbons, whereas the Pt-catalyzed C−C bond scission, i.e., hydrogenolysis, which occurs usually at 300−450 °C and gives high yields of methane and ethane (cf. Table 2),[28−32] is obviously of little contribution, given the low quantities of C_{1-2} observed in this work. As such, the activity and selectivity for the tandem catalysis are not solely dependent on BAS or Pt density but the overall site density and the balance between Pt sites and acid sites.

The regulating effects of CeO_2 on the dispersion and chemical state of Pt species as well as the porosity and acid properties of the Pt-*n*Ce/HY catalysts, which are all vital factors for the metal−acid tandem catalysis, implied a large potential impact of CeO_2 on the catalytic performance of Pt-*n*Ce/HY catalysts in PO hydrocracking. The catalytic performance of a series of Pt-*n*Ce/HY catalysts was evaluated and displayed in Figure 6A. Both Pt-1Ce/HY and Pt-2Ce/HY gave a high yield of solid residue of ca. 78 wt %, which is greatly higher than that of Pt/HY, ca. 10 wt %. Such a by far lower activity upon the addition of 1 or 2 wt % Ce is attributed to the lower Pt dispersion (i.e., lower amount of active Pt sites (n_{Pt}); cf. Table 3) caused by surface occupancy by cerium oxide, which somewhat limits the rate of the initial PO dehydrogenation leading to a low overall activity.

At a higher Ce addition of 3 wt % (i.e., more generation of CeO_2), more surface oxygen vacancies were provided for adsorbing the Pt species, leading to higher Pt dispersion and improved the overall balance between Pt and acid sites (Tables 2 and 3). As a result, the Pt-3Ce/HY catalyst gave a rather high LDPE conversion, with only 5.1 wt % of solid residue and a high product selectivity of 96.1% (corresponding to a yield of 84.8 wt %) toward C_{5-12} gasoline-range hydrocarbons, which represents one of the highest levels compared with the literature results (cf. Table 1). Nevertheless, at higher Ce additions (i.e., 4, 5, and 11 wt %), the yield of the solid residue increased regardless of the improved Pt dispersion (Figure 6A), which is attributed to the limited BAS-catalyzed cracking reaction over the decreased BAS density, causing a lower overall activity for metal−acid tandem catalysis. In short of proper amounts of acid sites, Pt nanoparticles (alone) could not contribute substantially to C−C bond breaking, which turned to be the rate-determining step, as the metal-catalyzed monofunctional hydrogenolysis requires higher temperatures and longer reaction time (cf. Table 1).[33,39] Compared to Pt/HY, Pt-3Ce/HY catalyst gave a product distribution with similarly high chain branching but shifted to larger hydrocarbons (Figure 6B,C), which is due to the less significant cracking reactions over the lower BAS density with lower acid strength (Table 3 and Figure S9). Given that Pt-3Ce/HY

https://doi.org/10.1021/acssuschemeng.3c04163
ACS Sustainable Chem. Eng. 2024, 12, 5738−5752

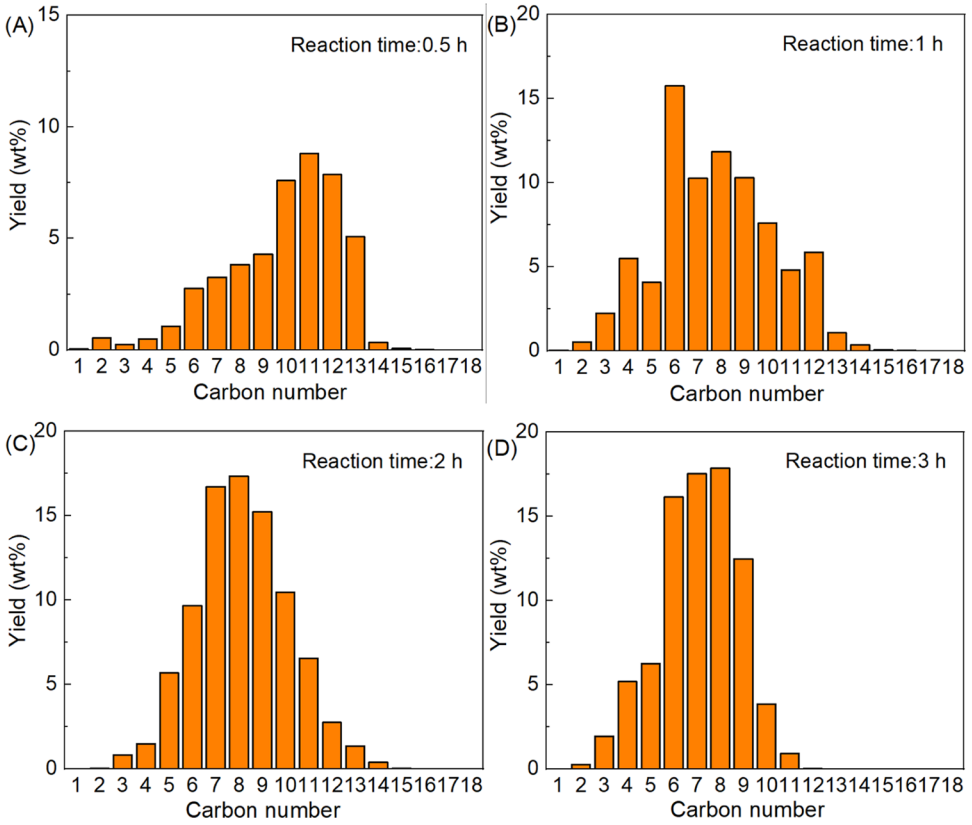

Figure 7. Product yield distribution by carbon number over Pt-3Ce/HY catalyst with a reaction time of (A) 0.5 h, (B) 1 h, (C) 2 h, and (D) 3 h. Reaction conditions: 280 °C, 2 MPa H_2, 200 mg of catalyst, and 2.0 g of PO. The solid residue yields of the reactions for 0.5, 1, 2, and 3 h are 38.1, 8.2, 5.1, and 4.5 wt %, respectively (cf. Table S4).

exhibited the highest LDPE conversion and maximum yield to gasoline-range hydrocarbons, it was selected as the optimized catalyst for follow-up studies.

Process conditions such as the reaction time, temperature, and H_2 pressure for the hydrocracking of LDPE were screened over the Pt-3Ce/HY catalyst for further process understanding and optimization (Figures 7−9 and Table S4). The effect of the reaction time on the product distribution is given in Figure 7 and Table S4 (entries 4−7). It was found that the LDPE conversion already reached a high level (with a solid residue yield of only 8.2 wt %) even after a short reaction time of 1 h. At prolonging reaction times of 2 and 3 h, the solid yield was further decreased, and the product distribution shifted logically to lighter hydrocarbons due to the deeper cracking (Figure 7). Almost no $C_{>15}$ product was observed in all cases, despite the fact that GC-FID was calibrated with up to C_{18}. Such a lack of heavier products is consistent with the literature studies for example, on a $Pt/WO_3/ZrO_2$ + HY zeolite catalyst blend for LDPE hydrocracking,[46] and is attributed to a preferential adsorption of long polymer chains over the intermediate hydrocarbons on the catalyst,[69] leading to a cracking process that proceeds with one polymer chain adsorbed and completely reacted without the release of medium-sized $C_{>15}$ products. Given the high LDPE conversion and desirable product selectivity toward C_{5-12} gasoline-range hydrocarbons, a reaction time of 2 h is selected for the subsequent reactions.

Temperature plays an important role in regulating the kinetics of the tandem catalysis for PO conversion, i.e., the relative rates of dehydrogenation/hydrogenation reactions, cracking reactions to C_{5-12} hydrocarbons, and C_{1-4} light gases, as well as side reactions such as coking. A general decreasing trend was observed in the yields of solid residues and relatively large hydrocarbons (e.g., C_{13-16}) with the increase of reaction temperature from 250 to 280 °C (Figure 8A and entries 5, 8−10 of Table S4). This is similar to the effect of increasing reaction time and because of the enhanced consecutive cracking of LDPE. Nevertheless, further increase of the temperature to 290 or 300 °C led to slightly higher yields of solid residue (entries 11 and 12 of Table S4; in line with the literature[42]), which is accompanied by a product distribution shifting to lighter hydrocarbons (e.g., decreased yield of C_{8-12} and increased yield of C_{5-7}; cf. Figure 8A). This indicates an enhancement of both the cracking and coking reactions over HY zeolites at these relatively higher temperatures above 280 °C, which is the characteristic of HY zeolite and regulated by both the acidity (Si/Al ratio) and diffusion constraints (meso/microporosity balance) thereof. The proposed higher generation of coke at a higher temperature >280 °C is supported by the thermogravimetric analysis (TGA)/differential scanning calorimetry (DSC) analysis on the recycled solid catalyst, which revealed a higher weight loss of 35.0% for the catalyst used at 300 °C vs 23.4% for that used at 280 °C (Figure S10). Moreover, the majority of the coke formed on the used Pt-3Ce/HY catalyst is believed to be hydrogen-rich or oxygen-containing coke, given that they are easily removed in the lower-temperature region below 300 °C (Figure S10). Generally, a reaction temperature of 280 °C was found to be optimal, given the lowest solid yield and desirable selectivity toward C_{5-12} hydrocarbons.

https://doi.org/10.1021/acssuschemeng.3c04163
ACS Sustainable Chem. Eng. 2024, 12, 5738−5752

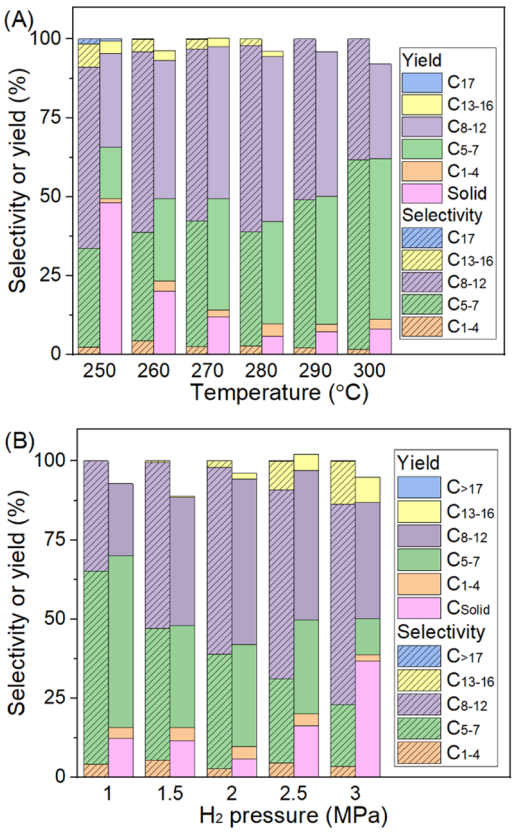

Figure 8. Product selectivity and yield from LDPE hydrocracking as a function of (A) temperature and (B) H_2 pressure. Reaction conditions (unless otherwise stated): Pt-3Ce/HY catalyst, 2 h, 280 °C, 2 MPa H_2, 200 mg of catalyst, and 2.0 g of PO.

The hydrogen pressure is also an important factor in the hydrocracking of PO, as it might affect the dehydrogenation/hydrogenation reaction equilibrium and even the acid properties of the catalysts.[46] The hydrocracking of LDPE was carried out under varying hydrogen pressure (P_{H_2}), and an optimal catalytic performance with the lowest yield of solid residue was found at a P_{H_2} of 2 MPa (Figure 8B). Similarly, Vlachos et al. reported an optimum P_{H_2} for LDPE hydrocracking over a $Pt/WO_3/ZrO_2$ + HY catalyst blend, and since the control experiments indicated an increase in the strength of the BAS on $Pt/WO_3/ZrO_2$ upon the hydrogen pretreatment, the lower LDPE conversion at lower P_{H_2} is believed to be possibly due to the lack of strong BAS.[46] However, in our case, a shift of the product distribution toward heavier hydrocarbons, e.g., a monotonous decrease in the yield of C_{5-7} but an increase in that of C_{8-12} and C_{13-16} hydrocarbons, was observed with the increase of P_{H_2} within the whole studied range from 1 to 3 MPa (Figure 8B), which is in contradiction with the deeper acid-catalyzed consecutive cracking over an increased strength of the acid sites at higher P_{H_2}. As such, the possible variation in the acid property should not be the reason for the lower activity at lower P_{H_2} (<2 MPa). Instead, we believe that the lower P_{H_2} might lead to a less significant hydrogenation of the olefin coke precursors, resulting in somewhat increased coking and thus the yield of the solid residue. In addition, mass transfer effect might also make a difference as the lower P_{H_2} tends to decrease the solubility and diffusion rate of H_2 in the polymer melt, slowing down the subsequent hydrocracking reactions.[41]

At higher P_{H_2} (>2 MPa), the increase in the yields of solid residue and the larger hydrocarbons (C_{8-12} and C_{13-16}), i.e., a decline of the catalytic performance with increasing P_{H_2}, is observed. This is attributed to a shift in the reversible dehydrogenation/hydrogenation (i.e., alkane/olefin conversion) equilibrium and a consequent decrease in the amount of active olefin intermediates, as dehydrogenation constitutes the initializing step of PO hydrocracking via the tandem metal−acid catalysis.[42] Moreover, saturation of the active sites on the catalyst with adsorbed hydrogen and suppressed H_2 desorption from the active sites under high P_{H_2} could also inhibit the deep cracking of the intermediates.

Catalytic Hydrocracking of Other Polyolefins (PP, HDPE, and Waste Plastic Bag). A notable challenge in the recycling of waste plastic is that the plastic products are usually multicomponent, particularly in the packaging industry, and as such, the development of catalysts and processes that are capable of treating multiple plastics (mixtures) are of importance. In this work, the present catalytic system was extended to the hydrocracking of other polyolefins such as HDPE, PP, and commercial plastic bags (HDPE) at 280 °C, 2 MPa H_2 for 2 h (Figure 9A). It was found that the Pt-3Ce/HY catalyst effectively converted all other plastics into the gasoline-range C_{5-12} liquid fuels in high yields (60−80 wt %; Figure 9B,C). The catalytic performance with PP was comparable to that with LDPE, with the product distribution falling more in the lighter products such as C_{1-4} and C_{5-7} hydrocarbons. This is attributed to the tertiary carbon environments on PP that are most capable of stabilizing the positive charge, as such compounds with ternary carbon are more prone to generate carbocation intermediates and crack over zeolites.[70,71] This explanation also applied to the higher solid yield, i.e., lower activity with HDPE, which has less chain branching compared to LDPE. The daily plastic bag (consisting mainly of HDPE) gave an even lower conversion than HDPE granules, which is attributed to the presence of additives such as stabilizers and dyes that have somewhat hindered the activity. However, a close to full conversion (5.7 wt % solid) was still achieved with a gasoline (C_{5-12}) yield of 82.7 wt %, given an extension of the reaction time to 12 h (Figure 9B). Generally, the slight difference in the catalytic performance on different plastics is related to the difference in their C−C bond strength and polymer backbone structure, and the current catalytic system over Pt-3Ce/HY represents an efficient process for the selective conversion of different polyolefin plastics into valuable C_{5-12} gasoline-range liquid fuels.

Stability and Reusability of the Pt−Ce/HY Catalyst. In addition to activity and selectivity, the stability and reusability of the catalysts are also of great importance for the potential implementation of the large-scale chemical recycling of waste polyolefins. For comparison, the reusability of Pt/HY and Pt-3Ce/HY was evaluated by running three consecutive reactions under optimized conditions (280 °C, 2 MPa H_2 and 2 h; cf. Figure 10). The used catalyst after each run was recycled via filtration, regenerated by calcination at 400 °C in air (according to the TGA/DSC results shown in Figure S10), and subsequently reduced in a H_2 flow (50 mL/min) at 300 °C for 4 h. The absence of the characteristic peaks of C−H stretching vibrations at 2800−3000 cm^{-1} in the IR spectra of the recalcinated Pt-3Ce/HY samples indicated a complete

https://doi.org/10.1021/acssuschemeng.3c04163
ACS Sustainable Chem. Eng. 2024, 12, 5738−5752

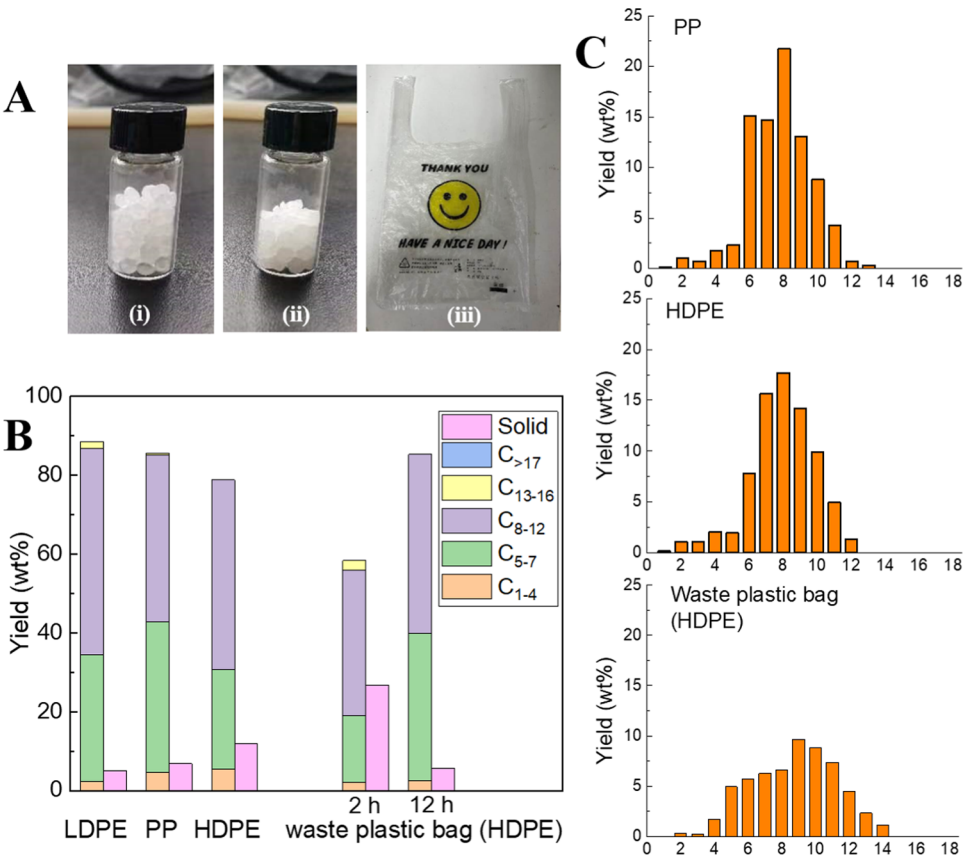

Figure 9. Hydrocracking of other polyolefin feedstocks. (A) (i) PP granules, (ii) HDPE granules, and (iii) plastics bag (HDPE). (B) Yield distribution of extractable products and solids for different polyolefins. (C) Product distribution by carbon number for different polyolefins over Pt-3Ce/HY. Reaction conditions: 280 °C, 2 MPa H_2, 2 h, 200 mg of catalyst, and 2.0 g of PO.

removal of the hydrocarbon residue upon regeneration (Figure S9). Despite the desirable activity and selectivity at the first run, the Pt/HY catalyst displayed distinct performance loss, e.g., the yield of the solid residue increased from 7.1 to 55.5 wt % after three reaction runs, with a general trend of product distribution shifting to heavier C_{8-12} hydrocarbons (Figure 10A). The possible reasons for such an activity loss could be (i) a declined Pt dispersion due to the migration and agglomeration of Pt atoms and (ii) decreased crystallinity and acidity of the HY zeolite caused by the leaching of Al or Si. Both reasons might impose a negative impact on the balance between Pt-catalyzed dehydrogenation and acid-catalyzed cracking reactions. To study the reason for catalyst deactivation, CO chemisorption and Pyridine-IR have been performed on the second-regenerated Pt/HY catalysts (Table S5). It is revealed that the Pt dispersion of Pt/HY decreased by ca. 50% upon three reaction runs, from 19.5 to 10.3%; and the BAS density of Pt/HY decreased apparently from 279.1 to 206.1 μmol/g (Table S5). Therefore, the main reason for the deactivation of Pt/HY is the loss of Pt dispersion and the BAS density; the latter also led to a product distribution shifting to heavier C_{8-12} hydrocarbons (Figure 10). The resulting insufficiency of Pt sites and BAS might cause not only a lower initial conversion rate but also a more severe coking that tends to deposit on the active sites, accelerating the catalyst deactivation.

Comparatively, Pt-3Ce/HY exhibited by far better stability and reusability, with a limited increase of solid yield from 5 to <10 wt % and a similar product distribution (mainly C_{5-12} hydrocarbons) after three reaction runs (Figure 10B). The dispersion of Pt on Pt-3Ce/HY was found to decrease only to a much smaller extent than that on Pt/HY, from 23.9 to 21.6%, and the BAS density slightly decreased from 152.6 to 141.2 μmol/g (Table S5). Such a higher stability (especially in the Pt dispersion) is attributed to the strong interaction between Pt and Ce forming a stable Pt−O−Ce bridging structure, which inhibited the migration, aggregation, and growth of the Pt particles during the reaction. The slight decrease in Pt dispersion could take place during the regeneration, where Pt atoms might migrate because of the well-known high volatility of PtO_2,[72] leading to somewhat increased Pt particle size. The XRD patterns of the fresh and regenerated Pt-3Ce/HY catalysts all displayed characteristic peaks of HY zeolites (Figure S12), indicating no severe structure collapse after reaction or regeneration, which is also supported by the similar morphology of the fresh and regenerated samples, as revealed by SEM (Figure S13). However, a slight decrease in peak intensity, i.e., a decrease of HY zeolite unit cell size, was observed for the regenerated samples. This is due to a lower Al content in the framework caused by a partial zeolite dealumination during regeneration,[46,73] which might lead to a small acidity decrease. Generally, despite the slightly decreased Pt dispersion and acidity, the regenerated Pt-3Ce/HY catalyst still afforded a desirable metal−acid balance, as reflected in similar product distributions among different reaction runs.

https://doi.org/10.1021/acssuschemeng.3c04163
ACS Sustainable Chem. Eng. 2024, 12, 5738−5752

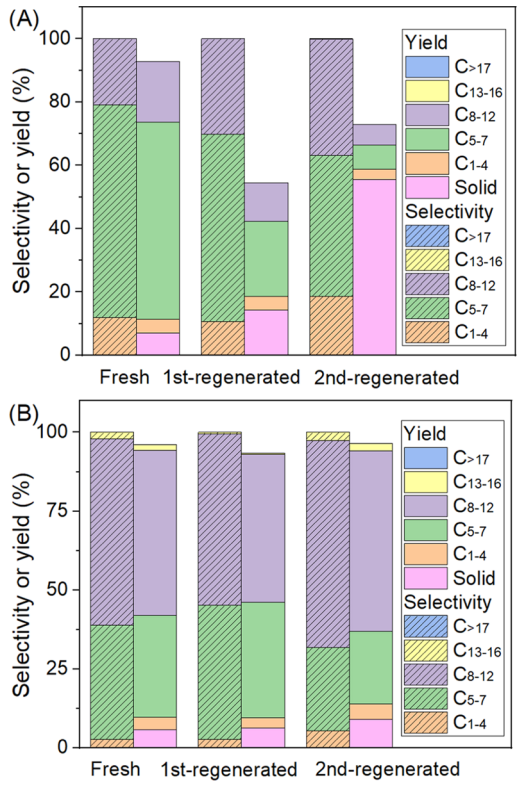

Figure 10. Evaluation of the reusability of (A) Pt/HY and (B) Pt-3Ce/HY. Reaction conditions: 280 °C, 2 MPa H_2, 2 h, 200 mg of catalyst, and 2.0 g of PO; regeneration conditions: calcination at 400 °C in air for 3 h and subsequently reduced in a H_2 flow (50 mL/min) at 300 °C for 4 h.

CONCLUSIONS

This work presented a highly selective process for the hydrocracking of (waste) polyolefins toward a spectrum of branched gasoline-range C_{5-12} liquid fuel, using a series of cerium-promoted Pt/HY (i.e., Pt-*n*Ce/HY) as the metal−acid bifunctional catalysts. A custom-modified HY zeolite was used as the support, which was engineered with a hierarchical meso/microporosity and a moderated acidity to avoid the over-cracking of the intermediate hydrocarbons to light C_{1-4} gas products. Cerium was present as a surface cerium oxide phase, which alleviated the acidity of HY zeolite and provided abundant oxygen vacancies for Pt adsorption, leading to a significantly improved Pt dispersion. Under optimized reaction conditions and Pt/Ce loading, i.e., over Pt-3Ce/HY (with 0.5 wt % Pt and 3 wt % Ce) that affords a proper metal−acid balance, a high yield of C_{5-12} hydrocarbons up to 84.6 wt % was achieved from the low-density polyethylene at 280 °C, 2 MPa H_2 for 2 h. A mechanism was proposed on the hydrocracking of polyethylene via metal−acid tandem catalysis over Pt-3Ce/HY, where the reaction proceeds with an initial dehydrogenation of the polymer chain or large alkane over the Pt sites to produce a large olefin, which was subsequently isomerized to branched carbocation reaction intermediates over the Brønsted acid sites, followed by a rapid β-scission to produce shorter unsaturated polymer chains or lighter olefins; meanwhile, these olefin intermediates were hydrogenated in the hydrogen atmosphere over Pt sites to form the corresponding alkanes. The strong interaction between Pt and Ce via the stable Pt−O−Ce bridging structure inhibited the migration and agglomeration of Pt particles, which endowed the Pt-3Ce/HY catalyst with largely enhanced stability compared to that of Pt/HY, exhibiting minimal performance loss over three sequential reaction runs. The present catalyst and process are applicable to the conversion of other common polyolefin wastes such as high-density polyethylene, polypropylene, and daily plastic bags to gasoline-range fuels in desirable yields (60−80 wt %).

Generally, engineering the acidity and porosity of the HY zeolite support, combined with proper cerium promotion as demonstrated in this work, represents a promising approach to synthesize bifunctional metal−acid catalysts with enhanced Pt dispersion, suitable metal−acid balance, and good stability. The process reported here may serve as a proof of concept for the upcycling of waste plastics into value-added liquid fuels in a sustainable way.

ASSOCIATED CONTENT

Supporting Information

The Supporting Information is available free of charge at https://pubs.acs.org/doi/10.1021/acssuschemeng.3c04163.

Experimental section (material; catalyst synthesis; characterizations; catalytic hydrocracking; product collection, analysis; and calculations); gel permeation chromatography (GPC) and DSC analysis of fresh LDPE feedstock; N_2 adsorption−desorption isotherms and DFT pore size distributions of HY, Pt/HY, and Pt-*n*Ce/HY catalysts; HADDF-STEM images of Pt/HY and Pt-3Ce/HY catalysts; XPS spectra of Ce 3d on Pt-*n*Ce/HY catalysts; peak fitting parameters for XPS spectra of Pt 4f and Ce 3d; pyridine-IR analysis results of HY, Pt/HY, and Pt-*n*Ce/HY catalysts; mechanistic discussion on the hydrocracking of polyethylene over Pt-*n*Ce/HY catalysts; product distributions from LDPE hydrocracking under different conditions; TGA and DSC analysis of the used Pt-3Ce catalyst after reaction; IR spectra of the used and regenerated Pt-3Ce/HY catalyst; and Pt dispersion, BAS density, XRD patterns, and SEM images of fresh and regenerated Pt/HY and Pt-3Ce/HY catalysts (PDF)

AUTHOR INFORMATION

Corresponding Authors

Jian Zhou − *State Key Laboratory of Green Chemical Engineering and Industrial Catalysis, Shanghai Research Institute of Petrochemical Technology, SINOPEC Corp., Shanghai 201208, China*; Email: zhouj.sshy@sinopec.com

Zhenhao Xi − *State Key Laboratory of Chemical Engineering, East China University of Science and Technology, Shanghai 200237, China; Shanghai Key Laboratory of Multiphase Materials Chemical Engineering, East China University of Science and Technology, Shanghai 200237, China;* orcid.org/0000-0002-4747-126X; Email: zhhxi@ecust.edu.cn

Authors

Pengcheng Zhao − *State Key Laboratory of Chemical Engineering, East China University of Science and Technology, Shanghai 200237, China*

Wenze Guo − *State Key Laboratory of Chemical Engineering, East China University of Science and Technology, Shanghai 200237, China; Key Laboratory of Smart Manufacturing in Energy Chemical Process, Ministry of Education, East China*

https://doi.org/10.1021/acssuschemeng.3c04163
ACS Sustainable Chem. Eng. 2024, 12, 5738−5752

University of Science and Technology, Shanghai 200237, China; Large-Scale Energy Storage Section, Department of Process and Energy, Delft University of Technology, 2628 CB Delft, The Netherlands; orcid.org/0000-0002-0543-8242

Zhipeng Gui − *State Key Laboratory of Chemical Engineering, East China University of Science and Technology, Shanghai 200237, China*

Jie Jiang − *State Key Laboratory of Chemical Engineering, East China University of Science and Technology, Shanghai 200237, China*

Zhihua Zhu − *State Key Laboratory of Chemical Engineering, East China University of Science and Technology, Shanghai 200237, China*

Jin-Jin Li − *Shanghai Key Laboratory of Multiphase Materials Chemical Engineering, East China University of Science and Technology, Shanghai 200237, China;* orcid.org/0000-0003-1660-387X

Ling Zhao − *State Key Laboratory of Chemical Engineering, East China University of Science and Technology, Shanghai 200237, China; Shanghai Key Laboratory of Multiphase Materials Chemical Engineering, East China University of Science and Technology, Shanghai 200237, China;* orcid.org/0000-0001-5239-1152

Complete contact information is available at: https://pubs.acs.org/10.1021/acssuschemeng.3c04163

Author Contributions

#P.Z. and W.G. contributed equally to this work. P.Z.: Experiments, data analysis, methodology; W.G.: conceptualization, methodology, validation, data analysis, investigation, visualization, supervision, writing—original draft, writing—review and editing; Z.G.: experiments, data analysis; J.J., Z.Z., and J.-J.L.: supervision; L.Z., J.Z., and Z.X.: resources, funding acquisition, supervision, project administration.

Notes

The authors declare no competing financial interest.

■ ACKNOWLEDGMENTS

This research was financially supported by the National Natural Science Foundation of China (Nos. 21978089 and 22293064), the Program of Shanghai Academic/Technology Research Leader (No. 21XD1433000), and the Key Research and Development Program of Xinjiang Uygur Autonomous Region (No. 2022B01032-1).

■ REFERENCES

(1) Europe, P. *Plastics-the Facts 2022*, An analysis of European plastics production, demand and Waste Data: Belgium, 2022.

(2) Garcia, J. M.; Robertson, M. L. The future of plastics recycling. *Science* **2017**, *358* (6365), 870−872.

(3) Rahimi, A.; García, J. M. Chemical recycling of waste plastics for new materials production. *Nat. Rev. Chem.* **2017**, *1* (6), No. 0046.

(4) Guo, W.; Bruining, H. C.; Heeres, H. J.; Yue, J. Insights into the reaction network and kinetics of xylose conversion over combined Lewis/Brønsted acid catalysts in a flow microreactor. *Green Chem.* **2023**, *25*, 5878−5898, DOI: 10.1039/D3GC00153A.

(5) Guo, W.; Hensen, E. J. M.; Qi, W.; Heeres, H. J.; Yue, J. Titanium Phosphate Grafted on Mesoporous SBA-15 Silica as a Solid Acid Catalyst for the Synthesis of 5-Hydroxymethylfurfural from Glucose. *ACS Sustainable Chem. Eng.* **2022**, *10* (31), 10157−10168.

(6) Guo, W.; Bruining, H. C.; Heeres, H. J.; Yue, J. Efficient synthesis of furfural from xylose over HCl catalyst in slug flow microreactors promoted by NaCl addition. *AlChE J.* **2022**, *68* (5), No. e17606.

(7) Guo, W.; Kortenbach, T.; Qi, W.; Hensen, E.; Jan Heeres, H.; Yue, J. Selective tandem catalysis for the synthesis of 5-hydroxymethylfurfural from glucose over in-situ phosphated titania catalysts: Insights into structure, bi-functionality and performance in flow microreactors. *Appl. Catal., B* **2022**, *301*, No. 120800.

(8) Jia, L.; Evans, S.; van der Linden, S. Motivating actions to mitigate plastic pollution. *Nat. Commun.* **2019**, *10* (1), No. 4582.

(9) Yadav, G.; Singh, A.; Dutta, A.; Uekert, T.; DesVeaux, J. S.; Nicholson, S. R.; Tan, E. C. D.; Mukarakate, C.; Schaidle, J. A.; Wrasman, C. J.; Carpenter, A. C.; Baldwin, R. M.; Román-Leshkov, Y.; Beckham, G. T. Techno-economic analysis and life cycle assessment for catalytic fast pyrolysis of mixed plastic waste. *Energy Environ. Sci.* **2023**, *16*, 3638−3653, DOI: 10.1039/D3EE00749A.

(10) Almohamadi, H.; Alamoudi, M.; Ahmed, U.; Shamsuddin, R.; Smith, K. Producing hydrocarbon fuel from the plastic waste: Techno-economic analysis. *Korean J. Chem. Eng.* **2021**, *38* (11), 2208−2216.

(11) Predel, M.; Kaminsky, W. Pyrolysis of mixed polyolefins in a fluidised-bed reactor and on a pyro-GC/MS to yield aliphatic waxes. *Polym. Degrad. Stab.* **2000**, *70* (3), 373−385.

(12) Al-Salem, S. M.; Dutta, A. Wax Recovery from the Pyrolysis of Virgin and Waste Plastics. *Ind. Eng. Chem. Res.* **2021**, *60* (22), 8301−8309.

(13) López, A.; de Marco, I.; Caballero, B. M.; Laresgoiti, M. F.; Adrados, A. Influence of time and temperature on pyrolysis of plastic wastes in a semi-batch reactor. *Chem. Eng. J.* **2011**, *173* (1), 62−71.

(14) Kaminsky, W.; Kim, J.-S. Pyrolysis of mixed plastics into aromatics. *J. Anal. Appl. Pyrolysis* **1999**, *51* (1), 127−134.

(15) Sharma, B. K.; Moser, B. R.; Vermillion, K. E.; Doll, K. M.; Rajagopalan, N. Production, characterization and fuel properties of alternative diesel fuel from pyrolysis of waste plastic grocery bags. *Fuel Process. Technol.* **2014**, *122*, 79−90.

(16) Serrano, D. P.; Aguado, J.; Escola, J. M. Catalytic conversion of polystyrene over HMCM-41, HZSM-5 and amorphous SiO2−Al2O3: comparison with thermal cracking. *Appl. Catal., B* **2000**, *25* (2), 181−189.

(17) Maity, A.; Chaudhari, S.; Titman, J. J.; Polshettiwar, V. Catalytic nanosponges of acidic aluminosilicates for plastic degradation and CO2 to fuel conversion. *Nat. Commun.* **2020**, *11* (1), No. 3828.

(18) Lerici, L. C.; Renzini, M. S.; Pierella, L. B. Chemical Catalyzed Recycling of Polymers: Catalytic Conversion of PE, PP and PS into Fuels and Chemicals over H-Y. *Procedia Mater. Sci.* **2015**, *8*, 297−303.

(19) Aguado, J.; Serrano, D. P.; San Miguel, G.; Castro, M. C.; Madrid, S. Feedstock recycling of polyethylene in a two-step thermo-catalytic reaction system. *J. Anal. Appl. Pyrolysis* **2007**, *79* (1), 415−423.

(20) Serrano, D. P.; Aguado, J.; Escola, J. M.; Garagorri, E.; Rodrı x guez, J. M.; Morselli, L.; Palazzi, G.; Orsi, R. Feedstock recycling of agriculture plastic film wastes by catalytic cracking. *Appl. Catal., B* **2004**, *49* (4), 257−265.

(21) Uemichi, Y.; Nakamura, J.; Itoh, T.; Sugioka, M.; Garforth, A. A.; Dwyer, J. Conversion of Polyethylene into Gasoline-Range Fuels by Two-Stage Catalytic Degradation Using Silica−Alumina and HZSM-5 Zeolite. *Ind. Eng. Chem. Res.* **1999**, *38* (2), 385−390.

(22) Zhou, N.; Dai, L.; Lv, Y.; Li, H.; Deng, W.; Guo, F.; Chen, P.; Lei, H.; Ruan, R. Catalytic pyrolysis of plastic wastes in a continuous microwave assisted pyrolysis system for fuel production. *Chem. Eng. J.* **2021**, *418*, No. 129412.

(23) Selvam, E.; Kots, P. A.; Hernandez, B.; Malhotra, A.; Chen, W.; Catala-Civera, J. M.; Santamaria, J.; Ierapetritou, M.; Vlachos, D. G. Plastic waste upgrade to olefins via mild slurry microwave pyrolysis over solid acids. *Chem. Eng. J.* **2023**, *454*, No. 140332.

(24) Scheirs, J. G. M.; Kaminsky, W. *Feedstock Recycling and Pyrolysis of Wast Plastics: Converting Waste Plastics into Diesel and Other Fuels*; Wiley, 2006.

(25) Jia, X.; Qin, C.; Friedberger, T.; Guan, Z.; Huang, Z. Efficient and selective degradation of polyethylenes into liquid fuels and waxes under mild conditions. *Sci. Adv.* **2016**, *2* (6), No. e1501591.

(26) Ding, W.; Liang, J.; Anderson, L. L. Hydrocracking and Hydroisomerization of High-Density Polyethylene and Waste Plastic over Zeolite and Silica−Alumina-Supported Ni and Ni−Mo Sulfides. *Energy Fuels* **1997**, *11* (6), 1219−1224.
(27) Vollmer, I.; Jenks, M. J. F.; Roelands, M. C. P.; White, R. J.; van Harmelen, T.; de Wild, P.; van der Laan, G. P.; Meirer, F.; Keurentjes, J. T. F.; Weckhuysen, B. M. Beyond Mechanical Recycling: Giving New Life to Plastic Waste. *Angew. Chem., Int. Ed.* **2020**, *59* (36), 15402−15423.
(28) Flaherty, D. W.; Iglesia, E. Transition-State Enthalpy and Entropy Effects on Reactivity and Selectivity in Hydrogenolysis of n-Alkanes. *J. Am. Chem. Soc.* **2013**, *135* (49), 18586−18599.
(29) Flaherty, D. W.; Hibbitts, D. D.; Gürbüz, E. I.; Iglesia, E. Theoretical and kinetic assessment of the mechanism of ethane hydrogenolysis on metal surfaces saturated with chemisorbed hydrogen. *J. Catal.* **2014**, *311*, 350−356.
(30) Flaherty, D. W.; Hibbitts, D. D.; Iglesia, E. Metal-Catalyzed C−C Bond Cleavage in Alkanes: Effects of Methyl Substitution on Transition-State Structures and Stability. *J. Am. Chem. Soc.* **2014**, *136* (27), 9664−9676.
(31) Flaherty, D. W.; Uzun, A.; Iglesia, E. Catalytic Ring Opening of Cycloalkanes on Ir Clusters: Alkyl Substitution Effects on the Structure and Stability of C−C Bond Cleavage Transition States. *J. Phys. Chem. C* **2015**, *119* (5), 2597−2613.
(32) Hibbitts, D. D.; Flaherty, D. W.; Iglesia, E. Effects of Chain Length on the Mechanism and Rates of Metal-Catalyzed Hydrogenolysis of n-Alkanes. *J. Phys. Chem. C* **2016**, *120* (15), 8125−8138.
(33) Celik, G.; Kennedy, R. M.; Hackler, R. A.; Ferrandon, M.; Tennakoon, A.; Patnaik, S.; LaPointe, A. M.; Ammal, S. C.; Heyden, A.; Perras, F. A.; Pruski, M.; Scott, S. L.; Poeppelmeier, K. R.; Sadow, A. D.; Delferro, M. Upcycling Single-Use Polyethylene into High-Quality Liquid Products. *ACS Cent. Sci.* **2019**, *5* (11), 1795−1803.
(34) Zhang, F.; Zeng, M.; Yappert, R. D.; Sun, J.; Lee, Y.-H.; LaPointe, A. M.; Peters, B.; Abu-Omar, M. M.; Scott, S. L. Polyethylene upcycling to long-chain alkylaromatics by tandem hydrogenolysis/aromatization. *Science* **2020**, *370* (6515), 437−441.
(35) Nakaji, Y.; Tamura, M.; Miyaoka, S.; Kumagai, S.; Tanji, M.; Nakagawa, Y.; Yoshioka, T.; Tomishige, K. Low-temperature catalytic upgrading of waste polyolefinic plastics into liquid fuels and waxes. *Appl. Catal., B* **2021**, *285*, No. 119805.
(36) Conesa, J. A.; Font, R.; Marcilla, A. Comparison between the Pyrolysis of Two Types of Polyethylenes in a Fluidized Bed Reactor. *Energy Fuels* **1997**, *11* (1), 126−136.
(37) Milne, B. J.; Behie, L. A.; Berruti, F. Recycling of waste plastics by ultrapyrolysis using an internally circulating fluidized bed reactor. *J. Anal. Appl. Pyrolysis* **1999**, *51* (1), 157−166.
(38) Akubo, K.; Nahil, M. A.; Williams, P. T. Aromatic fuel oils produced from the pyrolysis-catalysis of polyethylene plastic with metal-impregnated zeolite catalysts. *J. Energy Inst.* **2019**, *92* (1), 195−202.
(39) Tennakoon, A.; Wu, X.; Paterson, A. L.; Patnaik, S.; Pei, Y.; LaPointe, A. M.; Ammal, S. C.; Hackler, R. A.; Heyden, A.; Slowing, I. I.; Coates, G. W.; Delferro, M.; Peters, B.; Huang, W.; Sadow, A. D.; Perras, F. A. Catalytic upcycling of high-density polyethylene via a processive mechanism. *Nat. Catal.* **2020**, *3* (11), 893−901.
(40) Li, L.; Luo, H.; Shao, Z.; Zhou, H.; Lu, J.; Chen, J.; Huang, C.; Zhang, S.; Liu, X.; Xia, L.; Li, J.; Wang, H.; Sun, Y. Converting Plastic Wastes to Naphtha for Closing the Plastic Loop. *J. Am. Chem. Soc.* **2023**, *145* (3), 1847−1854.
(41) Jumah, A. B.; Anbumuthu, V.; Tedstone, A. A.; Garforth, A. A. Catalyzing the Hydrocracking of Low Density Polyethylene. *Ind. Eng. Chem. Res.* **2019**, *58* (45), 20601−20609.
(42) Liu, S.; Kots, P. A.; Vance, B. C.; Danielson, A.; Vlachos, D. G. Plastic waste to fuels by hydrocracking at mild conditions. *Sci. Adv.* **2021**, *7* (17), No. eabf8283.
(43) Hesse, N. D.; White, R. L. Polyethylene catalytic hydrocracking by PtHZSM-5, PtHY, and PtHMCM-41. *J. Appl. Polym. Sci.* **2004**, *92* (2), 1293−1301.
(44) Jumah, A. B.; Malekshahian, M.; Tedstone, A. A.; Garforth, A. A. Kinetic Modeling of Hydrocracking of Low-Density Polyethylene in a Batch Reactor. *ACS Sustainable Chem. Eng.* **2021**, *9* (49), 16757−16769.
(45) Pyra, K.; Tarach, K. A.; Śrębowata, A.; Melián-Cabrera, I.; Góra-Marek, K. Pd-modified beta zeolite for modulated hydrocracking of low-density polyethylene into a paraffinic-rich hydrocarbon fuel. *Appl. Catal., B* **2020**, *277*, No. 119070.
(46) Liu, S.; Kots, P. A.; Vance, B. C.; Danielson, A.; Vlachos, D. G. Plastic waste to fuels by hydrocracking at mild conditions. *Sci. Adv.* **2021**, *7* (17), No. eabf8283.
(47) Yang, F.; Zhong, J.; Liu, X.; Zhu, X. A novel catalytic alkylation process of syngas with benzene over the cerium modified platinum supported on HZSM-5 zeolite. *Appl. Energy* **2018**, *226*, 22−30.
(48) Shi, Y.; Li, Z.; Wang, J.; Zhou, R. Synergistic effect of Pt/Ce and USY zeolite in Pt-based catalysts with high activity for VOCs degradation. *Appl. Catal., B* **2021**, *286*, No. 119936.
(49) Resasco, J.; DeRita, L.; Dai, S.; Chada, J. P.; Xu, M.; Yan, X.; Finzel, J.; Hanukovich, S.; Hoffman, A. S.; Graham, G. W.; Bare, S. R.; Pan, X.; Christopher, P. Uniformity Is Key in Defining Structure−Function Relationships for Atomically Dispersed Metal Catalysts: The Case of Pt/CeO2. *J. Am. Chem. Soc.* **2020**, *142* (1), 169−184.
(50) Fuku, K.; Goto, M.; Sakano, T.; Kamegawa, T.; Mori, K.; Yamashita, H. Efficient degradation of CO and acetaldehyde using nano-sized Pt catalysts supported on CeO2 and CeO2/ZSM-5 composite. *Catal. Today* **2013**, *201*, 57−61.
(51) dos Santos, B. R. V.; Urbina, M. M.; Souza, M. J. B.; Pedrosa, A. M. G.; Silva, A. O. S.; Sobrinho, E. V.; Castedo, R. V. Preparation and characterization of Pt-dealuminated Y zeolite by TG/DTA and TPR. *J. Therm. Anal. Calorim.* **2015**, *119* (1), 391−399.
(52) Dvořák, F.; Camellone, M. F.; Tovt, A.; Tran, N.-D.; Negreiros, F. R.; Vorokhta, M.; Skála, T.; Matolínová, I.; Mysliveček, J.; Matolín, V.; Fabris, S. Creating single-atom Pt-ceria catalysts by surface step decoration. *Nat. Commun.* **2016**, *7* (1), No. 10801.
(53) An, K.; Alayoglu, S.; Musselwhite, N.; Plamthottam, S.; Melaet, G.; Lindeman, A. E.; Somorjai, G. A. Enhanced CO Oxidation Rates at the Interface of Mesoporous Oxides and Pt Nanoparticles. *J. Am. Chem. Soc.* **2013**, *135* (44), 16689−16696.
(54) Salaev, M. A.; Salaeva, A. A.; Kharlamova, T. S.; Mamontov, G. V. Pt−CeO2-based composites in environmental catalysis: A review. *Appl. Catal., B* **2021**, *295*, No. 120286.
(55) Borodziński, A.; Bonarowska, M. Relation between Crystallite Size and Dispersion on Supported Metal Catalysts. *Langmuir* **1997**, *13* (21), 5613−5620.
(56) Chen, Z.; Mao, J.; Zhou, R. Preparation of size-controlled Pt supported on Al2O3 nanocatalysts for deep catalytic oxidation of benzene at lower temperature. *Appl. Surf. Sci.* **2019**, *465*, 15−22.
(57) Tiernan, M. J.; Finlayson, O. E. Effects of ceria on the combustion activity and surface properties of Pt/Al2O3 catalysts. *Appl. Catal., B* **1998**, *19* (1), 23−35.
(58) Ye, X.; Wang, H.; Lin, Y.; Liu, X.; Cao, L.; Gu, J.; Lu, J. Insight of the stability and activity of platinum single atoms on ceria. *Nano Res.* **2019**, *12* (6), 1401−1409.
(59) Bêche, E.; Charvin, P.; Perarnau, D.; Abanades, S.; Flamant, G. Ce 3d XPS investigation of cerium oxides and mixed cerium oxide (CexTiyOz). *Surf. Interface Anal.* **2008**, *40* (3−4), 264−267.
(60) Thill, A. S.; Figueiredo, W. T.; Lobato, F. O.; Vaz, M. O.; Fernandes, W. P.; Carvalho, V. E.; Soares, E. A.; Poletto, F.; Teixeira, S. R.; Bernardi, F. New horizons in photocatalysis: the importance of mesopores for cerium oxide. *J. Mater. Chem. A* **2020**, *8* (46), 24752−24762.
(61) Soni, S.; Vats, V. S.; Kumar, S.; Dalela, B.; Mishra, M.; Meena, R. S.; Gupta, G.; Alvi, P. A.; Dalela, S. Structural, optical and magnetic properties of Fe-doped CeO2 samples probed using X-ray photoelectron spectroscopy. *J. Mater. Sci.: Mater. Electron.* **2018**, *29* (12), 10141−10153.
(62) Liu, L.; Shi, J.; Zhang, X.; Liu, J. Flower-Like Mn-Doped CeO2Microstructures: Synthesis, Characterizations, and Catalytic Properties. *J. Chem.* **2015**, *2015*, No. 254750.

https://doi.org/10.1021/acssuschemeng.3c04163
ACS Sustainable Chem. Eng. 2024, 12, 5738−5752

(63) Lafaye, G.; Barbier, J.; Duprez, D. Impact of cerium-based support oxides in catalytic wet air oxidation: Conflicting role of redox and acid−base properties. *Catal. Today* **2015**, *253*, 89−98.
(64) Liu, P.; Wang, J.; Zhang, X.; Wei, R.; Ren, X. Catalytic performances of dealuminated Hβ zeolite supported Pt catalysts doped with Cr in hydroisomerization of n-heptane. *Chem. Eng. J.* **2009**, *148* (1), 184−190.
(65) Hong, X.; Sun, Y.; Zhu, T.; Liu, Z. Promoting effect of TiO2 on the catalytic performance of Pt-Au/TiO2(x)-CeO2 for the co-oxidation of CO and H2 at room temperature. *Appl. Surf. Sci.* **2017**, *396*, 226−234.
(66) Guisnet, M.; Alvarez, F.; Giannetto, G.; Perot, G. Hydroisomerization and hydrocracking of n-heptane on Pth zeolites. Effect of the porosity and of the distribution of metallic and acid sites. *Catal. Today* **1987**, *1* (4), 415−433.
(67) Weitkamp, J. Catalytic Hydrocracking—Mechanisms and Versatility of the Process. *ChemCatChem* **2012**, *4* (3), 292−306.
(68) Akah, A.; Hernandez-Martinez, J.; Rallan, C.; Garforth, A. Enhanced Feedstock Recycling of Post-Consumer Plastic Waste. *Chem. Eng. Trans.* **2015**, *43*, 2395−2400.
(69) Vance, B. C.; Kots, P. A.; Wang, C.; Hinton, Z. R.; Quinn, C. M.; Epps, T. H.; Korley, L. T. J.; Vlachos, D. G. Single pot catalyst strategy to branched products via adhesive isomerization and hydrocracking of polyethylene over platinum tungstated zirconia. *Appl. Catal., B* **2021**, *299*, No. 120483.
(70) Corma, A.; Wojciechowski, B. W. The Chemistry of Catalytic Cracking. *Catal. Rev.* **1985**, *27* (1), 29−150.
(71) Bhan, A.; Gounder, R.; Macht, J.; Iglesia, E. Entropy considerations in monomolecular cracking of alkanes on acidic zeolites. *J. Catal.* **2008**, *253*, 221−224.
(72) Jones, J.; Xiong, H.; DeLaRiva, A. T.; Peterson, E. J.; Pham, H.; Challa, S. R.; Qi, G.; Oh, S.; Wiebenga, M. H.; Hernández, X. I. P.; Wang, Y.; Datye, A. K. Thermally stable single-atom platinum-on-ceria catalysts via atom trapping. *Science* **2016**, *353* (6295), 150−154.
(73) Arafat, A.; Jansen, J. C.; Ebaid, A. R.; van Bekkum, H. Microwave preparation of zeolite Y and ZSM-5. *Zeolites* **1993**, *13* (3), 162−165.

https://doi.org/10.1021/acssuschemeng.3c04163
ACS Sustainable Chem. Eng. 2024, 12, 5738−5752